Int. J. Electrochem. Sci., 10 **(2015)** 2377 - 2390

International Journal of ELECTROCHEMICAL SCIENCE
www.electrochemsci.org

Corrosion Performance of Nanostructured Clay Hybrid Film based on Crosslinked 3-(Acrylamidopropyl) Trimethylammonium Chloride –co- Acrylamide on Mild Steel in Acidic Medium

Ayman M. Atta[1,2], *Gamal A. El-Mahdy*[1,3], *Hamad A. Al-Lohedan*[1], *Ahmed M. Tawfeek*[4], *Shaban R. Sayed*[4]

[1] Department of Chemistry, Surfactant Research Chair, College of Science, King Saud University, Riyadh 11451, Saudi Arabia
[2] Petroleum application department, Egyptian petroleum research institute, Nasr city 11727, Cairo, Egypt.
[3] Chemistry department, Faculty of Science, Helwan University, Helwan 11795, Egypt
[4] College of Science, King Saud University, Riyadh, Saudi Arabia
*E-mail: khaled_00atta@yahoo.com

Received: 23 October 2014 / *Accepted:* 13 December 2014 / *Published:* 19 January 2015

The present work describes the exfoliation of clay through crosslinking with 3- (acrylamidopropyl) trimethylammonium chloride–co- acrylamide (APTAC/AM) which made the polymer end-tethered on Na-MMT. However, the way in which APTAC/AM interacts with the surface of MMT has not yet been studied. APTAC/AM widened the gap between clay layers and facilitates comonomers penetrate into clay. The exfoliated structure of extracted nanocomposite was confirmed by Fourier transform infrared (FTIR), X-ray powder diffraction XRD, thermogravimetric analyses (TGA) and transmission electron microscopy (TEM). Results of FT-IR, TGA and XRD analyses showed that APTAC/AM interacted with clay, but to various extents. The inhibition effect of APTAC/AM-MMT on the corrosion of steel in 1.0 M HCl solution was studied by potentiodynamic polarization curves and electrochemical impedance spectroscopy (EIS) methods. All electrochemical measurements indicate that APTAC/AM-MMT functioned as a good inhibitor in 1M hydrochloric solution and inhibition efficiency increased with APTAC/AM-MMT concentration. Polarization curves indicate that APTAC/AM-MMT acts as mixed-type inhibitor. EIS spectra exhibit one capacitive loop. The charge transfer resistance (Rct) increases with APTAC/AM-MMT concentration, while double layer capacitance (Cdl) decreases.

Keywords: Nanocomposite, clay hybrid film, 3- (acrylamidopropyl) trimethylammonium chloride–co- acrylamide, acid corrosion inhibition, steel, polarization, EIS.

1. INTRODUCTION

Recently, significant efforts and challenges have been directed to produce highly protected metallic surfaces to corrosive environments. Apart from most of the corrosion protection alternatives, self-healing protection technologies are highly reliable, since they are widely used to prevent corrosion of metallic structures [1-4]. Prior to the function of inhibitor particles, high dispersity of the polymer is attained by the support materials [5–7] and the use of nano-size particles leads to advanced barrier function of composites [8, 9]. Dispersability problems [5] can be solved by the use of highly dispersed polymeric carrier supported [10, 11]. The inorganic-organic hybrid materials can adapt to the environment, change wettability and adhesion to the surface depending on the external conditions [12]. Recently, great efforts have been focused on research to prepare hybrid materials with crosslinked mico- and nanogels [13-16]. Therefore, it is still challenging to find hybrid particles having superior properties such as surface activity, dispersability and self-assembly on the substrate surfaces for various applications. Montmorillonite, one of layered aluminosilicate minerals, can be used because of its unique physicochemical properties such as tunable large interlayer space [17]. Several types of crosslinked nanoparticle based on acrylamide polymers have been successfully introduced to the interlayer space within the anisotropic lamellar structure of montmorillonite [18, 19].

Polymeric quaternary ammonium compounds having unique properties attracted great attention to apply as anti- corrosive materials in various industrial processing for preventing corrosion of iron and steel in acidic media [20-22]. Therefore, they have been the subject of extensive investigations for several decades and still continue to be an active area of research. Although previous studies have clearly demonstrated that polymeric quaternary ammonium compounds act as an excellent kind of inhibitor for steel in acidic medium, they are rarely accepted in industrial application due to high-cost in comparison with conventional surfactants. One of the most useful strategies to reduce the cost is based on improve the performance of the corrosion inhibitors at low dose in the presence of hypride materials [23]. In the present work, we extend our works on nanocomposites [13-15, 18, 19] to increase the performance of polymeric quaternary ammonium compounds through crosslinking and introduce to the interlayer space of clay galleries. In this respect, (3-acrylamidopropyl) trimethylammonium chloride (APTAC) was chemically crosslinked after dispersion between clay layers to produce nanogel composite to apply as anti-corrosion self-assembled thin film on the mild steel substrate in acidic medium. The inhibition efficiencies of the prepared hybrid polymers were investigated using potentiodynamic polarization curves and electrochemical impedance spectroscopy (EIS).

2. EXPERIMENTAL

2.1. Materials:

Nanoclay (sodium montmorillonite; Na¯MMT) hydrophilic was purchased from Sigma-Aldrich Co. (St. Louis, MO, USA) with commercial name `Nanomer ® PGV. 3-

Acrylamidopropyl)trimethylammonium chloride solution (APTAC; 75 wt. % in H_2O), acrylamide (AM), poly(vinyl pyrrolidone) (PVP) with molecular weight 40,000 g/mol, *N*,*N*-methylenebisacrylamide (MBA), ammonium persulfate (APS), and *N*,*N*,*N*′,*N*′-tetramethylethylenediamine (TEMED) were obtained from Sigma Chemicals (St Louis, MO, USA). All reagents were used as received, and double deionized (DDI) water prepared with a UVO ultrapurification system (Millipore, Billerica, MA, USA) was used throughout the work. The sample (working electrode) was selected from a steel rod with a chemical composition (in wt%) as follows: 0.14% C, 0.57% Mn, 0.21% P, 0.15% S, 0.37% Si, 0.06% V, 0.03% Ni, 0.03% Cr and and the and Fe as balance. The electrode was abraded with SiC abrasive papers of different grades (200, 400, 600, 800, 1000 and 1200, 2000) then washed in bi-distilled water degreased ultrasonically in ethanol, and finally dried at room temperature before being immersed in the test solutions. The test solution, 1.0 M HCl was prepared by dilution of analytical grade 37% HCl with double distilled water.

2.2. Preparation of APTAC/AM-MMT nanocomposite:

The nanocomposite was synthesized using free radical copolymerization of APTAC and AM monomers in the presence of MBA as a crosslinker. In 500 mL round-bottom flask, 7 g of Na-MMT and 1 g PVP were dispersed with 300 mL of EtOH/H_2O (60/40 vol %). The solution was stirred at room temperature for 24 h. The flask was purged with nitrogen and 0.0125 g KPS initiator (dissolved in 3ml H_2O) and 20 µl TEMED were added to the mixture. The monomers AM (0.5 g; 7 mmol) and APTAC (1.91 g; 7 mmol) and 0.144 g of MBA (6 Wt % based on monomers concentration) were successively introduced at room temperature under stirring. The polymerization was allowed to proceed at 45 °C for 24 h. The produced APTAC/AM-MMT nanocomposite separated after ultracentrifuge at 21000 rpm for 30 minute and washed four times with EtOH/H_2O and vacuum dried at 30 ^{o}C.

Purification of APTAC/AM-MMT nanocomposite was carried out by extraction small amount of nanocomposites with THF in a Soxhlet extractor for 12 h to remove oligomers or water molecules. The extracted APTAC/AM-MMT nanocomposite was dried under a highly reduced pressure at 100 ^{o}C for 50 h and molded to disc type at nominal 3000 psi of pressure.

2.3. Characterization

Fourier transform infrared (FTIR) spectrometer (Nicolet, NEXUS-670) was used to elucidate the functional groups of the nanocomposite with a range 4000-400 cm^{-1} using KBr pellets.

TEM micrographs of colloidal nanocomposite particle were taken using a JEOL JEM-2100 electron microscope. A few drops of nanocomposite solution were diluted into 1 mL of ethanol, and the resulting ethanol solution was placed onto a carbon coated copper grid and allowed to evaporate. HR-TEM images of the nanocomposite were recorded using a JEM-2100F (JEOL) at an acceleration voltage of 200 kV.

Wide-angle X-ray diffraction study of the samples is performed on a Rigaku D/MAX-3C OD-2988N X-ray diffractometer with cooper target and Ni filter at a scanning rate of 4^o/min. The basal space of clay layers was calculated from X-ray patterns.

Thermogravimetric analysis (TGA) of the nanocomposites was carried out using a TGA-50 SHIMADZU thermogravimetric instrument, with a TA-50 WSI thermal analyzer. Samples (7 mg) were degraded in a nitrogen atmosphere (flow rate 50 ml/min) at a heating rate of 20 ◦C/min.

2.4. Electrochemical measurements:

The electrochemical studies were performed in a three electrode cell assembly. Steel samples were used as a working electrode. Platinum sheet was used as a counter electrode and saturated calomel electrode (SCE) as reference electrode. All the potentials were reported versus SCE. All electrochemical measurements were carried out using a Solartron 1470E system (Potentiostat/ Galvanostat) with Solartron 1455A as frequency response analyzer to perform all polarization and EIS measurements. Potentiodynamic polarization curves were conducted at a scan rate of 1 mV/s. EIS measurements were carried out in a frequency range from 10k Hz to 0.01 Hz. Polarization data were collected and analyzed using CorrView, CorrWare software. The analysis of impedance spectra and fitting of experimental results to equivalent circuits were performed using Zplot and ZView software.

3. RESULTS AND DISCUSSION

Clay minerals are characterized by their two-dimensional sheets (galleries) of corner sharing SiO_4 tetrahedral and/or AlO_4 octahedral. Clays can be categorized depending on the way that tetrahedral and octahedral sheets are packaged into layers. The clay layer will have no charge, or will have a net negative charge depending on the composition of the tetrahedral and octahedral sheets,. If the layers are charged this charge is balanced by interlayer cations such as Na^+ or K^+. In each case the interlayer can also contain water. Sodium montmorillonite (NaMt) is one of clay minerals and its particles are laminar in shape and their surface charge is not homogeneously distributed: face surfaces bear a negative charge generated by substitution of lattice ions and hence essentially independent of the composition of the aqueous medium, and edge surfaces have a pH-dependent charge [23]. The crosslinking of monomers between clay sheets is one of the most effective methods used to exfoliate the clay layers to increase their efficiency and to produce dispersed clay colloid nanoparticles [24]. In the present work, we selected ATAp monomer, having positive charges, to diffuse between clay galleries due to difference between ATAP and clay sheet charges. The crosslinking of ATAP and AM monomers in the presence of MBA crosslinker among Na-MMT sheets via cationic exchange interactions with ATAP was illustrated in the scheme1. The crosslinked hybrid clay was prepared by the intercalation of organic species ATAP into layered inorganic solids contain properties of both the inorganic host and the organic guest in a single material [25].

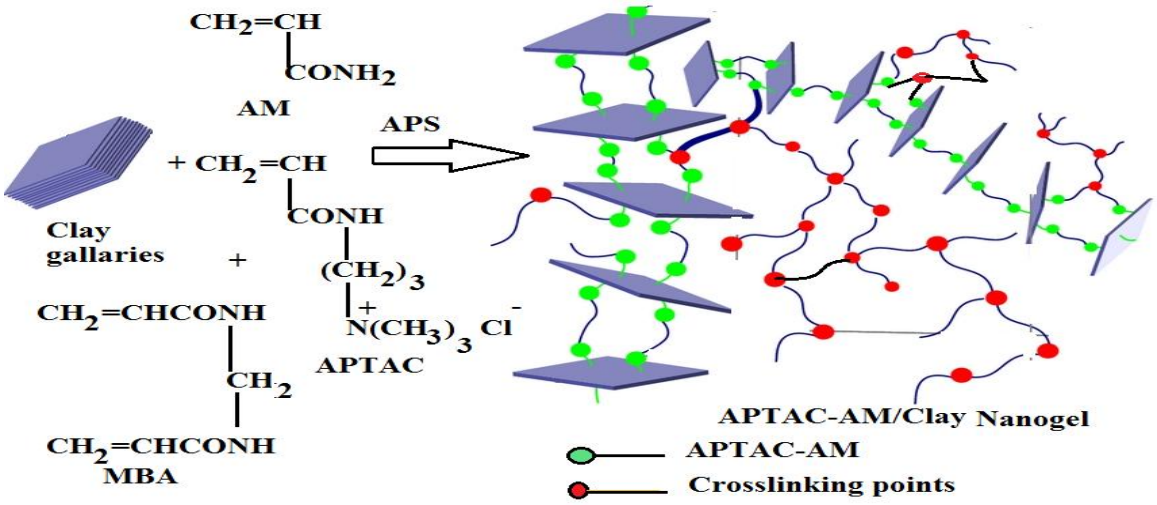

Scheme 1. Preparation of APTAC/AM-MMT.

3.1. Chemical structure and morphology of APTAC/AM-MMT

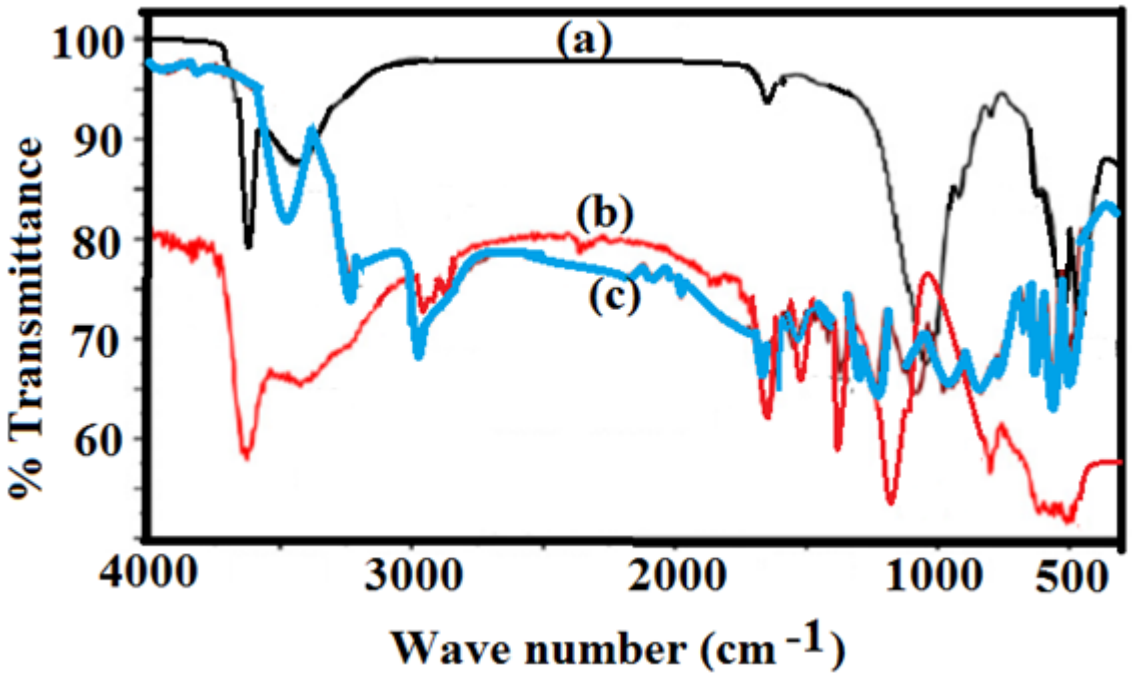

Figure 1. FTIR spectra of a) Na-MMT, b) APTAC/AM and c) APTAC/AM-MMT.

The chemical structures of the prepared composites based on APTAC/AM-MMT were confirmed by FTIR analysis. The FTIR spectra were represented in Figure 1. The FT-IR spectrum of Na-MMT (Figure 1a) shows absorption bands at 3430, 3630 and 1640 cm^{-1}, which referred to the OH stretching of the clay silicate layers [26]. The Si–O bond stretching showed narrow band at 1043 cm−1 which confirmed the silicate layer [26]. Moreover, the band at 620 cm^{-1} is referred to the Al–O of the silicate layers. The IR spectrum of the crosslinked polymer particles(Figure 1b) shows the

characteristic absorption bands (APTAC/AM) at 3485 cm^{-1}, and 1646 cm^{-1} (amide CONH stretching) and the characteristic bands of AM at 3290 cm−1, and the characteristic peak of MBA at 1381 cm^{-1}. The appearance of these bands in the FT-IR spectrum of APTAC/AM-MMT (figure 1c) indicates the presence of APTAC/AM in the clay. The bands at 2947 and 2850 cm^{-1} are related to C–H stretching of APTAC/AM molecules. However, FT-IR at least confirms the presence of APTAC/AM in clay after washing five times.

The TEM image was used to study the morphology of APTAC/AM-MMT to illustrate the intercalation and exfoliation of Na-MMT. In the respect TEM image of APTAC/AM-MMT was illustrated in Figure 2. The TEM data indicated that the dispersability of APTAC/AM-MMT in aqueous solution showed different morphologies. The flocculated structure having particle diameter ranged from 5 to 8 nm observed for this composite. The small intercalated clay was also observed via aggregates. The smaller Na-MMT particles were dispersed and adsorbed around the APTAC/AM particles, and they formed the "strawberry" structure [27]. This implies that the crosslinking polymerization process of APTAC/AM monomer obtains enough elastic force for exfoliation of the clay. The intercalated clay was effectively interacted with APTAC/AM because of the necessity for the charge counterbalance of the clay interlayers.

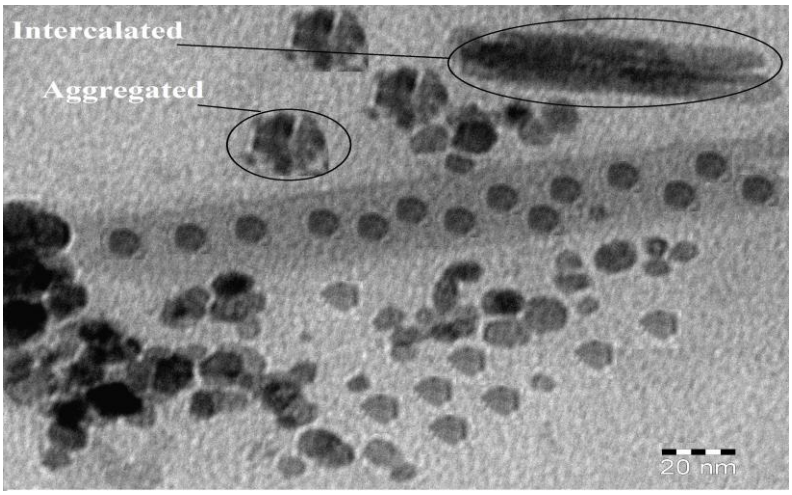

Figure 2. TEM micrograph of APTAC/AM-MMT composite.

3.2. Organization of APTAC/AM in the Na-MMT

The organization of APTAC/AM in the Na-MMT galleries can be determined from changes in the interlayer distance of Na-MMT and position of interplanner distance of (001) reflection plane which determined from XRD measurements. The XRD patterns of APTAC/AM polymers, Na-MMT, and APTAC/AM-MMT were illustrated in Figure 3. The *d*-spacing is calculated according to Bragg's law, namely $2d_{001} \sin \theta = \lambda$ (where θ is the diffraction angle and λ is the wavelength value corresponds to the associated Bragg peak position). The peak of Na- MMT dispersed in water occurs at 5.78 corresponding to the basal space of 1.55 nm in 2θ value, which means interlayer space of silicate is widened by water [28]. Moreover, the Na-MMT dispersed with APTAC/AM comonomers in water

shows the peak around 8.78 with the d001-space of 1.27 nm. The shift of peak position from 5.78 to 8.78 confirms the exchange of clay Na^+ with APTAC/AM to intercalate of APTAC/AM comonomers among Na-MMT galleries [29]. The APTAC/AM -MMT shows no peak which indicate that APTAC/AM intercalated in clay to exfoliate the clay layers.

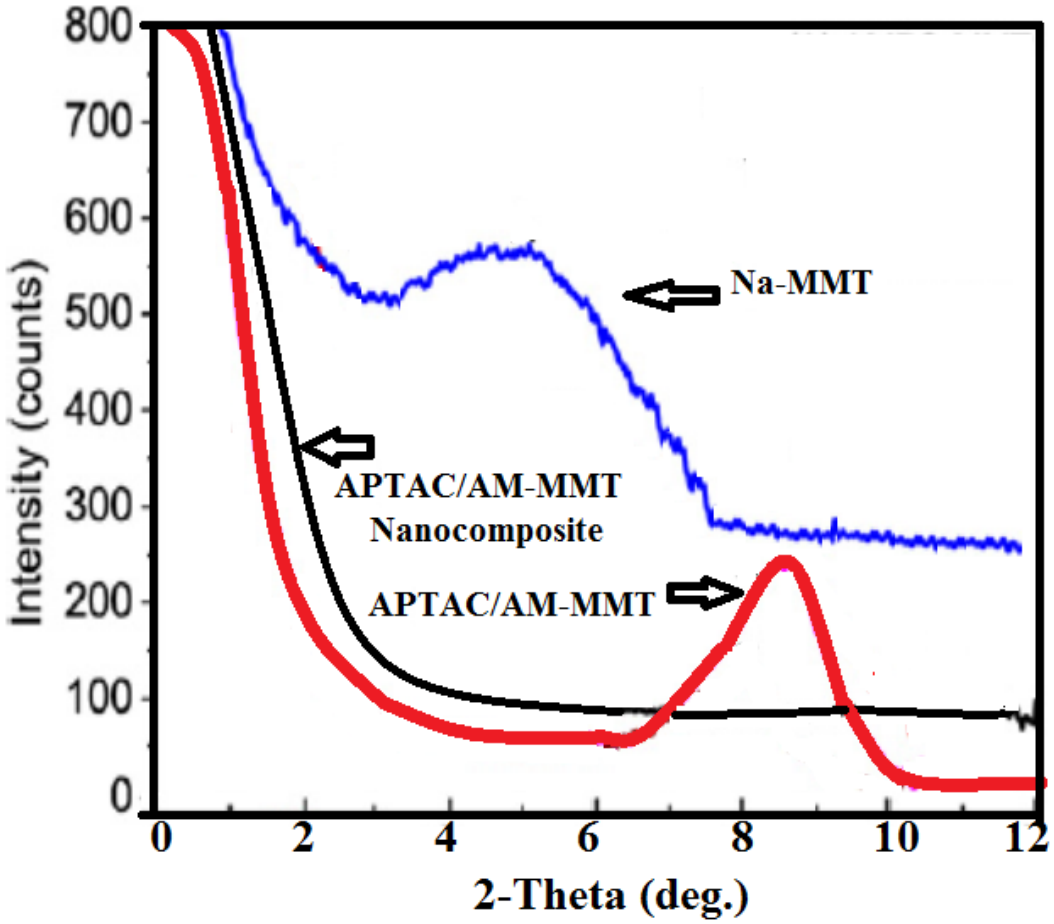

Figure 3. XRD diffractograms of Na-MMT, APTAC/AM and APTAC/AM-MMT.

Thermogravimetric analysis (TGA) is commonly used to determine the amount of polymers intercalated in clay galleries. In this respect, The TGA thermograms of the crosslinked APTAC/AM polymers, Na-MMT, and APTAC/AM-MMT were represented in figure 4. The Na-MMT losses about 4 % (Wt %) from its initial weight at temperature ranged from 50 to 100 ^oC which can be referred to loss of absorbed water. Moreover APTAC/AM polymers showed two degradation steps. The first degradation step was occurred between 50 and 100 ^oC due to the loss of water. The second degradation step occurred between 250 and 330 ^oC which can be referred to degradation of amide group chains to ammonia and water. The amount of APTAC/AM loaded in the clay galleries was determined from the difference between the residual weight difference between Na-MMT and APTAC/AM –MMT at 600 ◦C (cf. Figure 4). The data indicated that 35 wt % of APTAC/AM were intercalated and adsorbed between clay galleries. This result agrees with the theoretical amount of both APTAC and AM

monomers. It can be concluded that APTAC/AM interacted positively charged organic molecules via the ion-exchange mechanism which occurs quantitatively, as reported for interaction of clay with cetyltrimethylammonium bromide (CTAB) [30].

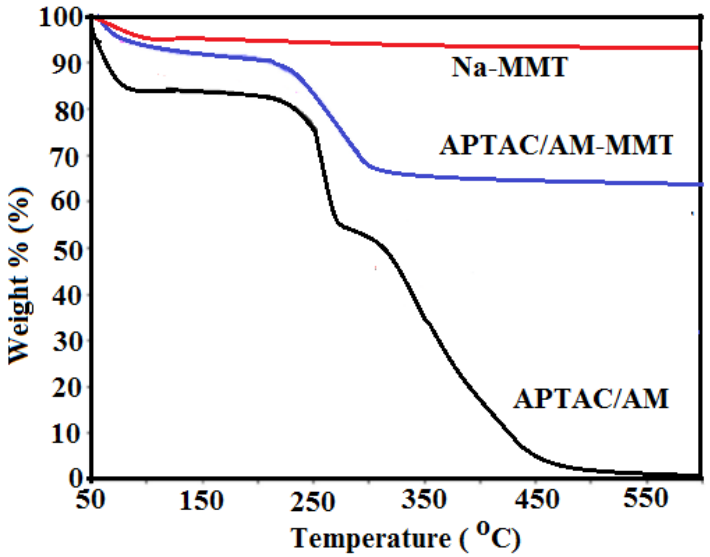

Figure 4. TGA thermograms of Na-MMT, APTAC/AM and APTAC/AM-MMT.

From the previous results it was expected that the modified clay gallery with high dispersion ability in aqueous water can be used as corrosion inhibitors. The proposed scheme for assembly of APTAC/AM-MMT on the steel surfaces was illustrated in scheme 2. It was expected that the positive charges of clay is driving force for assembly of clay galleries on the steel surfaces. Moreover, the nanocomposite film inhibits the diffusion of chloride ions towards steel [31] by forming an insulating and protective film, which protect the underlying steel from corrosion. .

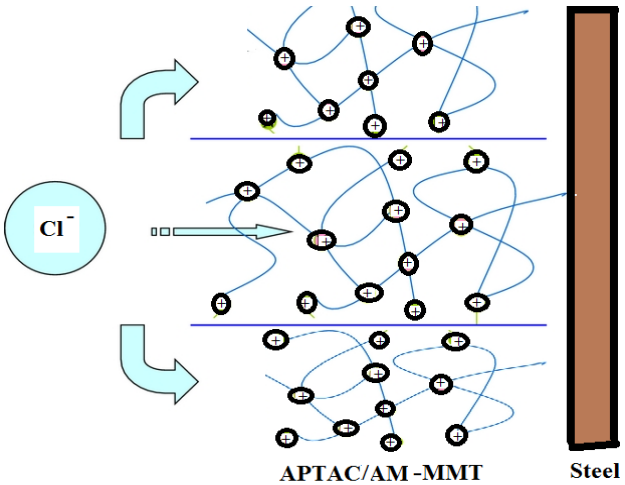

Scheme 2. Assembly of APTAC/AM-MMT at steel surface.

3.3. Polarization measurements

Potentiodynamic polarization curves for steel in 1.0 M HCl solution containing various concentrations of APTAC/AM-MMT is shown in Fig.5. It is clear that the addition of APTAC/AM-MMT to 1M HCl solution causes a prominent decrease in the corrosion rate i.e. shifts both anodic and cathodic curves to lower values of current densities as compared to the blank solution. These results indicate that APTAC/AM-MMT acts as a mixed-type inhibitor. The inhibition action can accounted to the reduction of the reaction area on the surface of the corroding steel [32] and the inhibition action is caused by geometric blocking effect [32]. It can be concluded that the presence of APTAC/AM-MMT inhibits the reduction of H^+ ions by merely blocking the reaction sites of steel surface [33-38]. The electrochemical corrosion parameters of corrosion current (Icorr), corrosion potential (Ecorr), anodic Tafel slope (ba) and cathodic Tafel slope (bc) are listed in Table 1. Apparently, Icorr decreases considerably in the presence of APTAC/AM-MMT and decreases with increasing the inhibitor concentration.

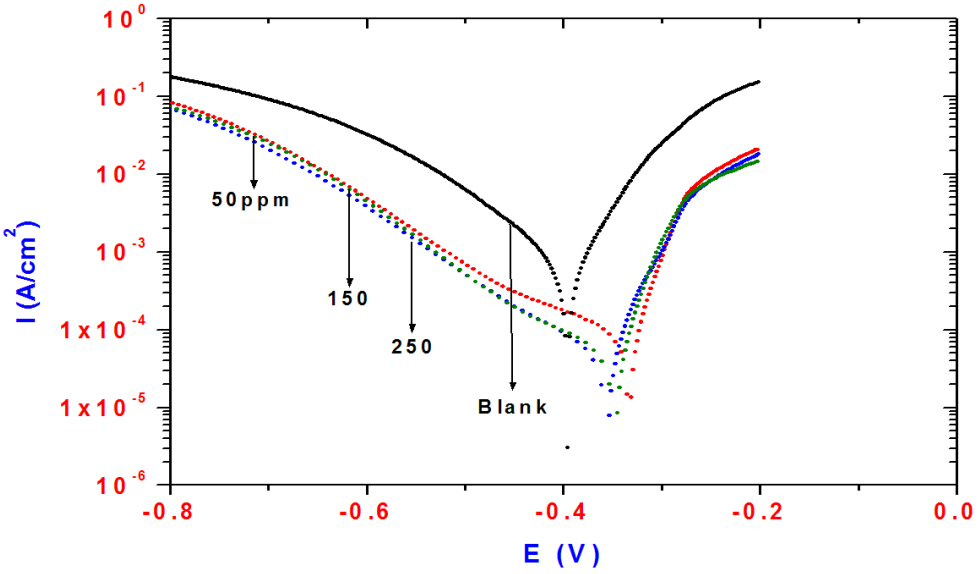

Figure 5. Polarization curves for steel in 1M HCl solution containing different APTAC/AM-MMT concentrations.

The results of Table show that the addition of APTAC/AM-MMT in HCl is accompanied by a change in the values of anodic (Ba), and cathodic (Bc), Tafel slopes slope as compared to the blank solution. This result suggests that the mechanism of steel dissolution and the reduction process underwent a modification when APTAC/AM-MMT are added. The inhibition efficiency was calculated using the following equation [39-40]:

$$IE\% = 1 - i_{corr\ (inh)} / i^{o}_{corr} \times 100 \quad (1)$$

Where $i_{corr\ (inh)}$ and i^{o}_{corr} are corrosion current densities in the presence and absence of inhibitor, respectively. The values of IE% with different inhibitor concentrations are listed in Table. Correspondingly, IE% increases with the inhibitor concentration, due to the increase in the blocked

fraction of the electrode surface by adsorption. IE% of 250 ppm inhibitor reaches up to the maximum of 92.8%, which indicates that APTAC/AM-MMT is a good inhibitor for steel in 1.0 M HCl. This can be explained by the formation of a more protective and compact film on the steel surface. The increase in inhibition efficiency indicates that a higher surface coverage was obtained in a solution with the optimum concentration of inhibitor (250ppm) due more adsorption of the APTAC/AM-MMT on the steel surface. This can be explained by the formation of a more protective and compact film on the steel surface. The results obtained by polarization curves show that the presence of APTAC/AM-MMT even in small concentration increases the resistance of the steel in the HCl solution. In addition, the data quoted in Table 1 shows that when the concentrations of APTAC/AM-MMT are increased, the values of corrosion current density decrease sharply, which associated with the increase in the inhibition efficiency. This indicates that the adsorptive film of APTAC/AM-MMT on steel surface becomes more perfect and stable with the increase in the concentrations of inhibitor.

Table 1. Inhibition efficiency values for steel in 1M HCl with different concentrations of APTAC/AM-MMT calculated by polarization and EIS methods.

Polarization Method						EIS Method		
	Ba (mV)	Bc (mV)	E_{corr} (V)	i_{corr} $\mu A/cm^2$	IE%	R_{ct} Ohm	Cdl ($\mu F/cm^2$)	IE%
Blank	69	120	-0.3955	839	_____	1.80	334	____
50ppm	57	272	-0.3469	82	90	17.9	114	89.9
150	58	114	-0.3552	77	91	19.8	113	90.9
250	47	159	-0.3338	60	93	25	108	92.8

3.4. Electrochemical impedance spectroscopy (EIS)

The Nyquist plots for steel in 1 M hydrochloric acid solution containing different concentrations of APTAC/AM-MMT are shown in Fig.6. The plot composed of one capacitive loop and the size increases with increasing concentration. The plots indicate that the dissolution process occurs under charge transfer control [41]. The diameter of the capacitive loop in the presence of inhibitor is bigger than that in the absence of inhibitor (blank solution) and increases with the inhibitor concentration. This indicates that the impedance of inhibited substrate increases with APTAC/AM-MMT concentration. The EIS results are fitted by an equivalent circuit consists of a solution resistance (Rs), a double layer capacitance (Cdl) in parallel with the charge transfer resistance (Rct). The electric models enable the calculation of numerical values corresponding to the physical and/or chemical properties of the electrochemical system under investigation [42]. The circuit employed allows the identification of charge transfer resistance (Rct) and the double layer capacitance (Cdl). The values of Rct and Cdl, for steel in 1 M hydrochloric acid solution containing different concentrations of APTAC/AM-MMT are presented in Table 1. Inspection of Table 1 reveals that Rct

values increases prominently while Cdl reduces with the concentration of APTAC/AM-MMT. Rct is associated with the corrosion resistance, so the higher charge transfer resistance indicates better inhibition performance. The decrease in Cdl comparing with that in blank solution (without inhibitor), which can result from a decrease in local dielectric constant and/or an increase in the thickness of the electrical double layer, suggests that the inhibitor function by adsorption at the steel/solution interface [43]. The inhibition efficiency (%IE) for the impedance data was estimated by comparing the charge transfer resistances (Rct) in the absence and presence of APTAC/AM-MMT as follows:

$$IE\% = 1 - R1_{ct}/R2_{ct} \times 100 \quad (2)$$

where $R1_{ct}$ and $R2_{ct}$ are the charge transfer resistances in absence and presence of the inhibitors, respectively. The values of IE% at different inhibitor concentrations are given in Table 1.

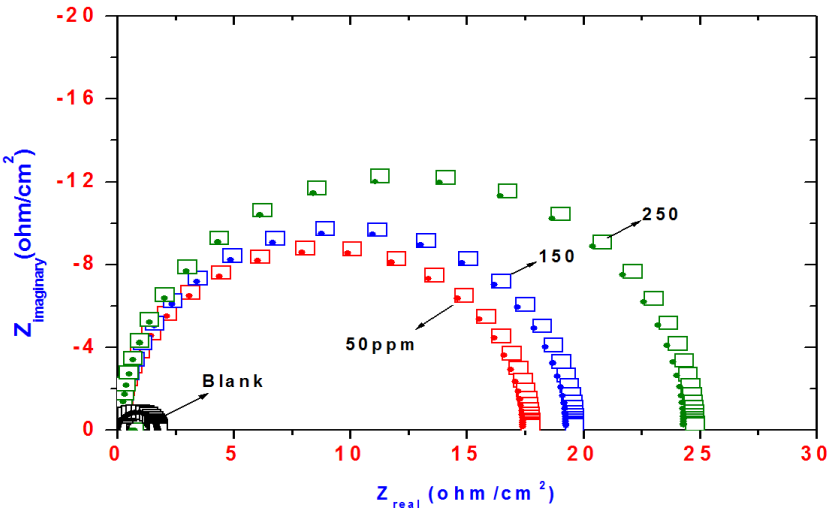

Figure 6. Nyquist diagram for steel in 1 M HCl solution containing APTAC/AM-MMT with different concentrations showing experimental (square) and fitted data (circle).

IE% increases with the concentration of APTAC/AM-MMT and reaches up to 92.8% at 250 ppm, which further confirm that APTAC/AM-MMT exhibits good inhibitive performance for steel in 1.0 M HCl. As the inhibitor concentration increased, the Cdl values tend to decrease while the Rct value and inhibition efficiency increase. This suggests that inhibitor molecules are absorbed on the steel surface and protect its surface from corrosion. Table 1 also shows that inhibition efficiencies (IE%) obtained from potentiodynamic polarization curves and EIS are in good reasonably agreement.

The adsorbed inhibitor on steel surface retards the cathodic and anodic electrochemical corrosion reaction. It has been reported that the mechanism of inhibition of an inhibitor may vary with factors such as inhibitor concentration, nature of the metal and nature of the acid anion [44]. Basic information on the interaction between the inhibitor and the steel surface can be provided by the adsorption isotherm. The degree of surface coverage (θ) values have been evaluated and plotted as function of the concentration of the inhibitor (C) and was tested graphically by fitting it to various isotherms to find the best fit, which describes the present work. Langmuir adsorption isotherm was

found to give the best description for APTAC/AM-MMT on steel as shown in Fig. 7 . This isotherm can be represented as [45]:

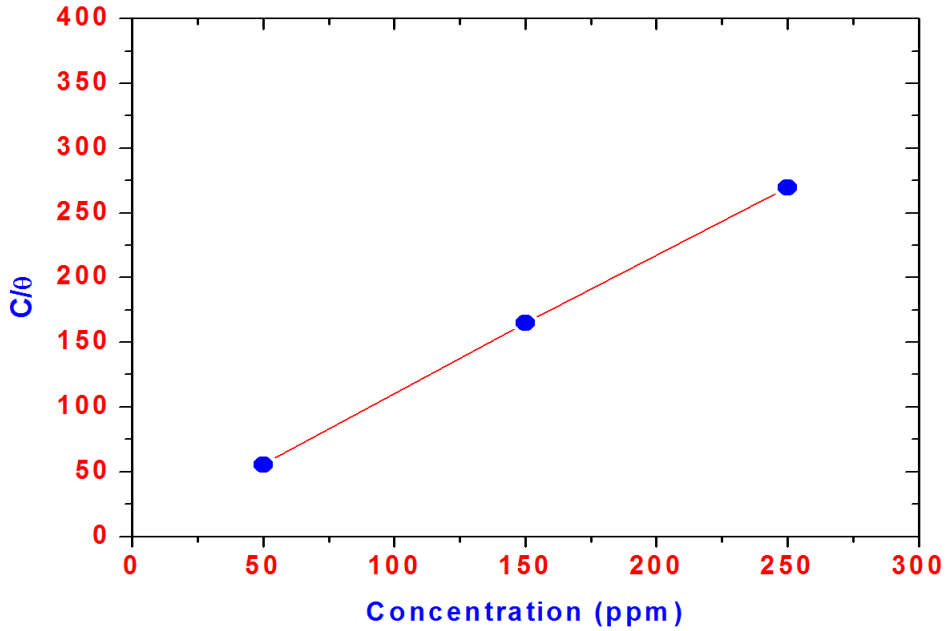

Figure 7. Langmuir's isotherm adsorption model of APTAC/AM-MMT on steel surface in 1 M HCl solution.

$$C_{(inh)} / \theta = 1/K_{ads} + C_{(inh)} \quad (3)$$

Where $C_{(inh)}$ is inhibitor concentration and Kads is the equilibrium constant for the adsorption process. A plot of C/ θ versus C (Fig.) gives a straight line with an average correlation coefficient of 0.9999 and a slope of nearly unity (1.068) suggests that the adsorption of APTAC/AM-MMT on steel obeys Langmuir adsorption isotherm. The value K_{ads} calculated from the reciprocal of intercept of isotherm line as 0.9355×105M−1. The high value of the adsorption equilibrium constant reflects the high adsorption ability of APTAC/AM-MMT on steel surface.

4. CONCLUSIONS

1. The FTIR, TEM and XRD data indicated the exfoliation of clay Na-MMT using cationic crosslinked APTAC/AM.
2. All electrochemical measurements indicate that APTAC/AM-MMT functioned as a good inhibitor in 1M hydrochloric solution and inhibition efficiency increased with APTAC/AM-MMT concentration.
3. APTAC/AM-MMT acts as a mixed inhibitor

4. EIS spectra exhibits one capacitive loop and the charge transfer resistance (Rct) is significantly increased, while double layer capacitance (Cdl) is markedly decreased with the APTAC/AM-MMT concentration.

5. Inhibition efficiencies (IE%) obtained from potentiodynamic polarization curves and EIS are in good reasonably agreement.

ACKNOWLEDGEMENTS
The authors extend their appreciation to the Deanship of Scientific Research at King Saud University for funding this work through research group no. RGP-VPP-235.

References

1. S.J. Garcia, H.R. Fischer, *Smart Polymers and their Applications*, Woodhead Publishing, Sawston, Cambridge, UK (2014) 271-298.
2. I.J. Zvonkina, M. Hilt, *Handbook of Smart Coatings for Materials Protection*, Woodhead Publishing, Sawston, Cambridge, UK (2014) 105-120.
3. K.A. Yasakau, M.G.S. Ferreira, M.L. Zheludkevich, H. Terryn, J.M.C. Mol, Y. Gonzalez-Garcia, Rare Earth-Based Corrosion Inhibitors, Woodhead Publishing, Sawston, Cambridge, UK (2014) 233-266.
4. J. Asadi, N.G. Ebrahimi, M. Razzaghi-Kashani, *Composites Part A: Applied Science and Manufacturing,* 68 (2015) 56.
5. M. Tiitu, A. Talo, O. Forse´n, O. Ikkal, *Polymer,* 46 (2005) 6855.
6. A. Malinauskas, *Polymer*, 42 (2001) 3957.
7. M. Ionita, A. Pruna, *Prog. Org. Coat*., 72 (2011) 647.
8. R. N. Rothon, *Adv. Polym. Sci*., 139 (1999) 67.
9. D. R. Paul, L. M. Robeson, *Polymer*, 49 (2008) 3187.
10. R. Partch, S. G. Gangolly, E. Matijevic, W. Cai, S. Arajs, *J. Colloid Interface Sci*., 144(1991) 27.
11. S. Maeda, S. P. Armes, *J. Mater. Chem.*, 4 (1994) 935.
12. *E. V. Skorb, D. V. Andreeva, Adv. Funct. Mater., 23* (2013) 4483.
13. G. A. El-Mahdy, A. M. Atta, H. A. Al-Lohedan, *Journal of the Taiwan Institute of Chemical Engineers*, 45 (2014) 1947.
14. A. M. Atta, G. A. El-Mahdy, H. A. Al Lohedan,A. O. Ezzat, *Molecules*, 19 (2014) 6246.
15. G. A. El-Mahdy, A. M. Atta, H. A. Al Lohedan, *Molecules*, 19(2014) 1713.
16. O. Zubillag, F.J. Cano, I. Azkarate, I.S. Molchan, G.E. Thompson, A.M. Cabral, P.J. Morais, *Surface & Coatings Technology*, 202 (2008) 5936.
17. Y-H. Son, J-K. Lee, Y.Soong, D. Martello, M. Chyu, *Chem. Mater.*, 22 (2010) 2226.
18. A. M. Atta, G. A. El-Mahdy, H. A. Al Lohedan, A.M. Tawfeek, *Digest Journal of Nanomaterials and Biostructures*, 9 (2014)531.
19. A. M. Atta, G. A. El-Mahdy, H. A. Al Lohedan, S.A. Al-Hussain, *Digest Journal of Nanomaterials and Biostructures,* 9 (2014) 627.
20. W. Jaeger, J. Bohrisch, A. Laschewsky, *Progress in Polymer Science*, 35 (2010) 511.
21. S.A. Ali, M.T.Saeed, *Polymer*, 42 (2001)2785.
22. L. Niu, H. Zhang, F. Wei, *Appl. Surf. Sci.*, 252 (2005) 1634.
23. L-G. Qiu, Y. Wu, Y-M. Wang, X. Jiang, *Corros. Sci.*, 50 (2008) 576.
24. J. D. G. Dur´an, M. M. Ramos-Tejada, F. J. Arroyo, F. Gonz´alez-Caballero, *Journal of Colloid and Interface Science*, 229(2000)107.
25. J. Cui, Q. Wang, X. Chen, Q. Wei, *Nanoscale Research Letters*, 9(2014)378.

26. M. Xu, Y.S. Choi, Y.K. Kim, K.H. Wang, I.J. Chung, *Polymer*, 44 (2003) 6387.
27. H-W. Cui, G-B. Du**,** *Journal of Chemical Engineering and Materials Science*, 2(2011) 122.
28. M. Xu, Y.S. Choi, Y. K. Kim, K. H. Wang, I. J. Chung, *Polymer*, 44 (2003) 6387.
29. F. Piscitelli, P. Posocco, R. Toth, M. Fermeglia, S. Pricl, G. Mensitieri,, M. Lavorgn, *Journal of Colloid and Interface Science*, 351 (2010) 108.
30. L. Biasci, M. Aglietto, G. Ruggeri, F. Ciardelli, *Polymer*, 35 (1994) 3296.
31. E. Huttunen-Saarivirta, G.V. Vaganov, V.E. Yudin, J. Vuorinen, *Progress in Organic Coatings*, 76 (2013) 757– 767
32. C. Cao, *Corros. Sci*., 38 (1996) 2073.
33. 1. X. Li, S. Deng, H. Fu, G. Mu, *Corros. Sci.*, 51 (2009) 620.
34. J. Aljourani, K. Raeissi, M.A. Golozar, *Corros. Sci*., 51 (2009) 1836.
35. I. Ahamad, R. Prasad, M.A. Quraishi, *Corros. Sci*., 52 (2010) 3033.
36. G.E. Badr, *Corros. Sci*., 51 (2009) 2529.
37. M. El Azhar, B. Mernari, M. Traisnel, F. Bentiss, M. Lagrenee, *Corros. Sci*., 43 (2001) 2229.
38. R. Solmaz, *Corros. Sci*., 52 (2010) 3321–3330.
39. E. McCafferty, *Corros. Sci*., 47 (2005) 3202.
40. Q. Qu, L. Li, W. Bai, S. Jiang, Z. Ding, *Corros. Sci*., 51 (2009) 2423.
41. A.M. Abdel-Gaber, M.S. Masoud, E.A. Khalil, E.E. Shehata, *Corros. Sci*., 51 (2009) 3021.
42. A.R.S. Priya, V.S. Muralidharam, A. Subramania, *Corrosion*, 64 (2008) 541.
43. M. Lagrenée, B. Mernari, M. Bouanis, M. Traisnel, F. Bentiss, *Corros. Sci*., 44 (2002) 573.
44. H.D. Lece, K.C. Emregul, O. Atakol, *Corros. Sci*. 50 (2008) 1460.
45. M. Lebrini, F. Bentiss, H. Vezin, M. Lagrenee, Corros. Sci. 48 (2006) 1279.